

# Earth's Future

## RESEARCH ARTICLE

10.1029/2023EF004039

### Key Points:

- The idealized symmetric CO<sub>2</sub> removal forcing leads to a reversible but asymmetric Indian summer monsoon (ISM) onset
- The delayed onset of ISM during the ramp-down period is primarily dominated by the asymmetric and lagged slow process, which is associated with the long-term sea surface temperature change
- The slow process delays the ISM onset by enhancing the near-surface poleward land-sea moist static energy contrast, which subsequently weakens the monsoonal circulation

### Supporting Information:

Supporting Information may be found in the online version of this article.

### Correspondence to:

X. Qu and G. Huang,  
[quxia@mail.iap.ac.cn](mailto:quxia@mail.iap.ac.cn);  
[hg@mail.iap.ac.cn](mailto:hg@mail.iap.ac.cn)







### Citation:

Zhang, S., Qu, X., Huang, G., Hu, P., Zhou, S., & Wu, L. (2024). Delayed onset of Indian summer monsoon in response to CO<sub>2</sub> removal. *Earth's Future*, 12, e2023EF004039. <https://doi.org/10.1029/2023EF004039>

Received 9 AUG 2023

Accepted 20 JAN 2024

## Delayed Onset of Indian Summer Monsoon in Response to CO<sub>2</sub> Removal

Suqin Zhang<sup>1,2</sup> , Xia Qu<sup>1,3</sup> , Gang Huang<sup>1,2,4</sup> , Peng Hu<sup>5,6</sup> , Shijie Zhou<sup>2,3</sup> , and Liang Wu<sup>2,3</sup> 

<sup>1</sup>State Key Laboratory of Numerical Modeling for Atmospheric Sciences and Geophysical Fluid Dynamics, Institute of Atmospheric Physics, Chinese Academy of Sciences, Beijing, China, <sup>2</sup>University of Chinese Academy of Sciences, Beijing, China, <sup>3</sup>Center for Monsoon System Research, Institute of Atmospheric Physics, Chinese Academy of Sciences, Beijing, China, <sup>4</sup>Laboratory for Regional Oceanography and Numerical Modeling, Qingdao National Laboratory for Marine Science and Technology, Qingdao, China, <sup>5</sup>Yunnan Key Laboratory of Meteorological Disasters and Climate Resources in the Greater Mekong Subregion, Yunnan University, Kunming, China, <sup>6</sup>Department of Atmospheric Sciences, Yunnan University, Kunming, China

**Abstract** Understanding the response of the Indian summer monsoon (ISM) onset to CO<sub>2</sub> forcing is of utmost importance for rain-fed agriculture and water management. In this study, we utilized an idealized symmetric CO<sub>2</sub> removal scenario from the sixth phase of the Coupled Model Intercomparison Project to analyze the reversibility of monsoon onset. The results show that ISM onset is reversible but exhibits strong asymmetry: it undergoes minimal changes during the ramp-up phase, but experiences rapid postponement as the CO<sub>2</sub> begins to decline; Eventually, it is delayed more than 1 week when the CO<sub>2</sub> concentration is restored to the initial level. To investigate the possible underlying mechanisms, we decomposed the climate response to CO<sub>2</sub> forcing into the fast and slow processes. Notably, it is the enhanced slow response, which is driven by long-term sea surface temperature (SST) changes, that dominates the asymmetric response of ISM onset. This slow response delays the ISM onset by strengthening near-surface poleward land-sea moist static energy contrast, thereby weakening the lower-tropospheric monsoonal circulation. Based on the atmospheric component model simulations, we found that both the uniform SST change and patterned SST changes in the slow response contribute to the delay of ISM onset, but the latter plays a dominant role. Our results emphasize the importance of thoroughly assessing regional hydrological cycle features when designing the CO<sub>2</sub> removal pathways.

**Plain Language Summary** The 2015 Paris Agreement set a target to limit global warming to 2°C by the end of the 21st century, with a preference for achieving 1.5°C. Meeting this temperature goal requires the atmospheric CO<sub>2</sub> concentration to peak in this century and then start declining. It is crucial to understand whether the changes in the regional hydrological cycle can be reversed when we reach the global mean temperature goal. This study focuses on examining the responses of the Indian summer monsoon (ISM) onset to idealized CO<sub>2</sub> removal (CDR) forcing, in which the atmospheric CO<sub>2</sub> concentration decreases symmetrically after increasing. Under the symmetric CDR pathway, the ISM onset displays reversible yet asymmetric evolution, it significantly delays when the CO<sub>2</sub> concentration returns to the pre-industrial level. This asymmetric response is attributed to the slow process of the climate system driven by long-term sea surface temperature change, which leads to the delay in ISM onset by weakening the lower-tropospheric circulation and, consequently, the precipitation. The slow response lags behind the evolution of CO<sub>2</sub> concentration and plays a dominant role in the global mean surface temperature change during the ramp-down phase. Understanding these mechanisms is essential for addressing climate change challenges and the impacts on regional monsoonal systems.

## 1. Introduction

Since the Industrial Revolution, massive greenhouse gas emissions, mainly carbon dioxide (CO<sub>2</sub>), induced by human activities have caused widespread climate change. The global mean surface temperature increased by 1.1°C in 2011–2020 compared to the pre-industrial (PI) level (IPCC, 2021). Particularly, the land where human beings live is extensively warmed by 1.6°C. Continuous warming leads to more frequent and intense weather and climate extremes across the globe, such as heatwaves, rainstorms, and droughts, which pose colossal threats to

natural ecosystems and human societies (Tang et al., 2022; X. Zhang et al., 2023). To reduce the risks posed by global warming and ensure sustainable development, several ambitious and feasible efforts, including “The Paris Agreement,” are now being considered. According to scientific estimation, the future CO<sub>2</sub> emissions pathways that limit the temperature increase to well below 2°C or 1.5°C proposed by the Paris Agreement by the end of this century require net negative CO<sub>2</sub> emissions (Iyer et al., 2022; Rogelj et al., 2018; Sanderson et al., 2017). The CO<sub>2</sub> removal (CDR), namely, the artificial removal of CO<sub>2</sub> from the atmosphere to achieve net negative CO<sub>2</sub> emissions, is proposed as a potential means (Field & Mach, 2017; Wang et al., 2021). However, there is a lack of comprehensive agreement on how the climate system under the CDR pathway would be. How does the reversibility of the climate system behave? Therefore, a comprehensive analysis is desired to assess the climate effects of CDR (G. Huang et al., 2022).

As a part of Coupled Model Intercomparison Project phase six (CMIP6), the Carbon Dioxide Removal Model Intercomparison Project was sponsored (Keller et al., 2018). Typically, an idealized CDR pathway is prescribed in which the atmospheric CO<sub>2</sub> concentration increases by 1% per year until it quadrupled relative to the PI level, and then it recovers along the mirror pathway to its initial concentration (Figure S1 in Supporting Information S1). Under this common framework, a series of studies have been undertaken to explore the climate response to CDR (Kim et al., 2022; Kug et al., 2022; Mondal et al., 2023; Zhou et al., 2022). As summarized in IPCC AR6 (IPCC, 2021), many global-scale climate phenomena, such as temperature, precipitation, and sea level, are irreversible. Namely, they cannot restore to their original state even though the atmospheric CO<sub>2</sub> concentration returns to the PI level. Particularly, most areas of the world would experience stronger hydrological cycles during the CDR periods due to the heat accumulated in the deep oceans (Wu et al., 2010; Yeh et al., 2021). However, the Indian summer monsoon (ISM) rainfall, as demonstrated by previous studies, is an exception (Wu et al., 2014; S. Zhang et al., 2023). Under the idealized CDR pathway, the ISM rainfall is largely reversible: it may overshoot the PI level and show a deficiency when CO<sub>2</sub> recovers.

With a local population of over 1 billion, ISM activities have significant and remarkable impacts on the socio-economic well-being of the region (Jin & Wang, 2017; Singh et al., 2019). The seasonal march of the ISM is characterized by three key stages: onset, peak, and demise, all of which exhibit notable variations (Bombardi et al., 2020; Hu et al., 2022). Although the peak summer rainfall (June–September) is widely recognized, changes in the onset of the ISM also have profound societal and economic implications. The onset of the ISM marks the arrival of the rainy season in India, which is critical for initiating agricultural cultivation and ensuring food security. Early or late onset of the ISM is strongly correlated with the widespread excess or deficit of seasonal rainfall across the ISM region (Misra et al., 2017; Noska & Misra, 2016). For instance, the delayed onset of ISM in 2014 resulted in a severe drought in Indian Peninsula, with a 12% reduction in precipitation (Kakatkhar et al., 2017; Pai & Bhan, 2014). Furthermore, the Tibetan Plateau, often referred to as the “Asian water tower,” is greatly influenced by the summer monsoon system (Yao et al., 2013; Zhu et al., 2020). Anomalous water vapor convergence caused by changes in the monsoonal circulation can impact precipitation over the Tibetan Plateau and inner lake area, as well as the water availability downstream in Asia (Liu et al., 2019; W. Zhang et al., 2017). The disparity in precipitation over the southeastern Tibetan Plateau between early and late ISM onset years is up to 23.41% of the climatology (Zhu et al., 2020). Considering the significant impacts of ISM onset on the ecosystem and human beings, it is essential to evaluate the climate effects of CDR on it.

The response of the climate system to CO<sub>2</sub> forcing involves various fundamental physical processes on different timescales, namely the rapid adjustment, and slow responses mediated by sea surface temperature (SST) warming (He & Zhou, 2022; T. Li et al., 2022). The rapid adjustment is the direct response of the land and atmosphere to the CO<sub>2</sub> radiative forcing, occurring within a timescale of less than 1 year (Mutton et al., 2022). On the other hand, the slow responses can be further divided into two processes associated with short- and long-term SST warming, as the SST response evolves over time (Zappa et al., 2020). These processes represents distinct physical mechanisms and exerts diverse climate impacts on ISM onset. For instance, the rapid adjustment under the global warming scenario enhances the land-sea contrast (T. Li et al., 2022; X. Li & Ting, 2016) and weakens atmospheric stability over land (Chadwick et al., 2019), creating favorable circulation condition for the ISM onset. The slow SST-mediated processes increase the atmospheric moisture content but weaken the land-sea contrast (X. Li & Ting, 2016), resulting in a counteracting effect. Under the CDR scenario, the time-varying relative contributions of these multiple timescale processes lead to a complex climate response. Understanding the roles of these processes in the ISM onset helps identify key factors and the assessment of the climate impact of CDR on this phenomenon.

Here, this work aims to address the following issues: (a) How does the ISM onset respond to an idealized CDR pathway? Can CDR reverse the changes in the ISM onset under global warming? (b) By separating fast and slow processes, which process is mainly responsible for the aforementioned responses? What are the underlying mechanisms? The remainder of the paper is organized as follows: Section 2 describes the data and analysis methods utilized in this study. Section 3 investigates the robust changes in ISM onset and examines the factors contributing to these changes. Section 4 provides a summary of the findings and discusses the implications of this study.

## 2. Data and Methods

### 2.1. The Idealized CDR Pathway

The idealized CDR pathway consists of three coupled general circulation model (CGCM) simulations from the CMIP6: piControl, 1pctCO<sub>2</sub>, and 1pctCO<sub>2</sub>-cdr experiments. Detailed information regarding these experiments is summarized in Table S1 in Supporting Information S1. The piControl experiment aims to represent a near-equilibrium state of the climate system to climate forcing under the pre-industrial level, with the last 100 years utilized as a climatology (PI) and initial condition. The first 140 years of 1pctCO<sub>2</sub> and 1pctCO<sub>2</sub>-cdr experiments are combined to construct the idealized CDR pathway, and the evolution of CO<sub>2</sub> concentration is depicted in Figure S1 in Supporting Information S1. Consequently, the entire duration of the CO<sub>2</sub> forcing pathway spans 280 years (140 years each for the ramp-up and ramp-down), with Year 1 defined as the first year of the 1pctCO<sub>2</sub> experiment for convenience. Currently, eight CGCMs have participated in the idealized CDR simulation, and detailed information about them is presented in Table S2 in Supporting Information S1. For each CGCM, one realization member is employed. The output of each CGCM is interpolated into a common 1° × 1° horizontal grid using bilinear interpolation. The analysis is conducted on the results obtained by the Multi-Model Ensemble (MME) to remove the effects of internal variability. When analyzing daily data, a fixed year of 365 days is utilized, excluding the 29th day of February in a leap year. For the model with only 360 days a year, piecewise linear interpolation is applied to align them with the 365-day calendar.

### 2.2. Definition of Onset Date of the ISM

To investigate the evolution of the monsoon system, multiple methods have been proposed to determine the onset date of the ISM based on precipitation or wind conditions (Bombardi et al., 2020; Hu et al., 2022). The India Meteorological Department (IMD) originally defined the ISM onset subjectively as a sharp and sustained increase of rainfall over Kerala (Ananthakrishnan & Soman, 1988; Joseph et al., 1994). However, this definition was prone to “bogus” monsoon onset due to small-scale disturbances affecting local rainfall (Fasullo & Webster, 2003; Wang et al., 2009). Therefore, the IMD adopted several objective criteria in 2006, which considered not only the rainfall over Kerala, but also the establishment of the monsoonal southwesterly flow and the emergence of active convection (Joseph et al., 2006; Pai & Nair, 2009). These criteria effectively excluded bogus monsoon onset, as detailed in Joseph et al. (2006) and Pai and Nair (2009). However, the daily circulation data required by Pai and Nair (2009) were unavailable in the CDR simulations. Thus, we used another objective method (Noska & Misra, 2016) that only required daily precipitation data. This method defined the monsoon onset as the beginning of the rainy season (Bombardi et al., 2019, 2020), which occurred when the regionally averaged precipitation over India stabilized above the annual mean daily precipitation of the climatology (Noska & Misra, 2016). This method was also immune to small-scale or higher-frequency fluctuations, such as synoptic disturbances, and avoided bogus monsoon onsets (Karmakar & Misra, 2019; Noska & Misra, 2016). Moreover, this method captured the seasonal evolution of the ISM, including the seasonal reversal of a meridional temperature gradient and the seasonal evolution of the low-level southwesterlies over the Indian Ocean (Goswami & Xavier, 2005; Hu et al., 2023; Krishnamurti & Ramanathan, 1982; Yanai et al., 1992). Therefore, this definition was widely used (Karmakar & Misra, 2019; Misra et al., 2018; Zhu et al., 2020).

We begin by calculating the Indian rainfall, which is the spatial average (original uninterpolated model grids) of land precipitation within the domain of 7.5°–30.5°N and 73°–90°E (red rectangle in Figure 2). For a particular year  $m$ , the cumulative daily anomaly  $C'_m(i)$  of the Indian rainfall for the day  $i$  is computed as

$$C'_m(i) = \sum_{n=1}^i [D_m(n) - \bar{C}] \quad (1)$$

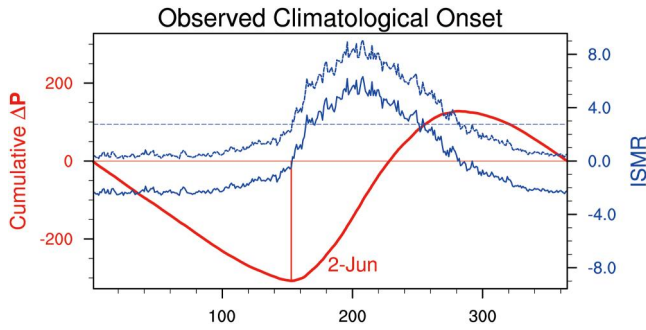


**Figure 1.** A schematic illustration of the time series of daily Indian rainfall (blue dashed line;  $D$  in Equation 1; units:  $\text{mm d}^{-1}$ ) and its anomalies (blue solid line) compared to the climatology (horizontal blue dashed line;  $\bar{C}$  in Equation 1). The red line represents the cumulative daily Indian rainfall anomaly ( $C'$  in Equation 1; units:  $\text{mm d}^{-1}$ ). The vertical red line indicates the onset date of the ISM (2 June) in observed climatology.

where

$$\bar{C} = \frac{1}{MN} \sum_{m=1}^M \sum_{n=1}^N D(m, n) \quad (2)$$

$D_m(n)$  represents the daily rainfall over India for day  $n$  of year  $m$ . The climatology  $\bar{C}$  is obtained by calculating the annual mean of the Indian rainfall over the  $N$  ( $=365$ ) days for  $M$  ( $=100$ ) years, using data from the last 100 years of the piControl experiments. The cumulative daily anomaly series have more stable trends than that of the raw Indian rainfall and are less susceptible to disturbances from small-scale systems (Hu et al., 2022; Noska & Misra, 2016). The onset date of the ISM is defined as the day when the cumulative daily anomaly  $C'_m(i)$  reaches its absolute minimum value, excluding the last 3 months of a year. To illustrate these variables, Figure 1 depicted the observed climatology with associated variables,  $D_m(n)$  and  $C'_m(i)$ . Since the daily rainfall anomalies over India (blue solid line) are

negative before the onset of ISM, their accumulation ( $C'_m(i)$ ; red line) shows a decreasing trend; after that, it exhibits a stable transition from negative to positive, and  $C'_m(i)$  shifts to an increasing trend. In the observed climatology, the onset date of the ISM is determined to be 2 June.

### 2.3. Definitions of Fast and Slow Responses

In line with previous studies (Monerie et al., 2021; Zhou et al., 2022; and many others), the response of the climate system to  $\text{CO}_2$  forcing can be understood as a linear combination of different timescale processes. These processes include rapid adjustment, which is related to the radiative forcing, and fast and slow responses mediated by SST changes. In this study, we combine the rapid adjustment and fast SST-mediated responses to form the total fast responses, while the slow responses are solely attributed to slow SST-mediated changes. To estimate these responses, we utilize the abrupt-4  $\times \text{CO}_2$  experiment, in which the  $\text{CO}_2$  concentration is abruptly increased to 4 times the pre-industrial level (Eyring et al., 2016). In the abrupt-4  $\times \text{CO}_2$  experiment, the global mean surface temperature experiences rapid warming primarily within the first 10 years. Subsequently, the rate of surface warming decreases rapidly and approaches 0 (Figure S2 in Supporting Information S1). Based on this behavior, we defined the fast response as the difference between the average of years 1–10 and PI, while the slow responses are defined as the difference between years 131–150 and years 1–10. This definition is consistent with previous studies (e.g., Zhou et al., 2022). The CGCMs used in this analysis are the same as those employed in the CDR experiments (see Table S2 in Supporting Information S1).

### 2.4. Contributions of Fast and Slow Responses Under CDR Scenario

In accordance with the approach outlined in Monerie et al. (2021) and Zappa et al. (2020), we estimated the contributions of the total fast and slow responses in the idealized CDR pathway based on their distinct patterns of surface warming. This approach assumes that the climate response scales directly with global surface warming and is independent of the background state of the climate. For a given year  $t$ , the surface warming responses  $\Delta T_{\text{CDR}}(t)$  can be regressed spatially (reshaped into a one-dimensional array, weighted by the cosine of the latitudes) on the normalized surface-warming patterns associated with the total fast and slow responses:

$$\Delta T_{\text{CDR}}(t) = F(t) \cdot \frac{\Delta T_{\text{fast}}}{\Delta T_{\text{fast}}} + S(t) \cdot \frac{\Delta T_{\text{slow}}}{\Delta T_{\text{slow}}} + r(t) \quad (3)$$

where the  $\Delta T_{\text{fast}}$  and  $\Delta T_{\text{slow}}$  represent the surface warming patterns of the total fast and slow responses obtained from the abrupt-4  $\times \text{CO}_2$  experiment, respectively. The overbar on these two terms denotes the global mean. Following the spatial multiple linear regression, the regression coefficients  $F(t)$  and  $S(t)$  represent the time-varying contributions of the total fast and slow responses, respectively, to global mean surface warming in the idealized CDR pathway. The intercept coefficient  $r(t)$  represents the residual warming pattern that is not linearly projected on these two timescales.

Using the regression coefficients  $F(t)$  and  $S(t)$ , the fast and slow responses of any variables in the CDR pathway can be reconstructed (Zhou et al., 2022). For a variable  $V$ , the reconstructed fast and slow responses ( $\Delta V_{\text{cdr\_fast}}(t)$  and  $\Delta V_{\text{cdr\_slow}}(t)$ ) can be expressed as

$$\Delta V_{\text{cdr\_fast}}(t) = F(t) \cdot \frac{\Delta V_{\text{fast}}}{\Delta T_{\text{fast}}} \quad (4)$$

$$\Delta V_{\text{cdr\_slow}}(t) = S(t) \cdot \frac{\Delta V_{\text{slow}}}{\Delta T_{\text{slow}}} \quad (5)$$

where the  $\Delta V_{\text{fast}}$  and  $\Delta V_{\text{slow}}$  represent the total fast and slow responses obtained from the abrupt-4  $\times$  CO<sub>2</sub> experiment, respectively.

## 2.5. The Idealized Atmosphere Component Model (AGCM) Experiments

Through the decomposition of the fast and slow responses, it has been observed that the slow response dominates the ISM onset response under the idealized CDR scenario, as discussed in Section 3.2. In order to investigate the potential mechanisms behind the slow responses influencing the ISM onset, a series of idealized AGCM simulations from the CMIP6 are analyzed (Webb et al., 2017). These simulations include the AMIP, AMIP-p4K, and AMIP-future4K, as outlined in Table S1 in Supporting Information S1. The AMIP-future4K experiment is compared with the AMIP experiment to ascertain the roles of total SST warming. Additionally, the effects of the total SST warming can be further divided into the effects of uniform SST change and patterned SST change. The former is represented by the difference between the AMIP-p4K and AMIP, while the latter is represented by the difference between AMIP-future4K and AMIP-p4K. Ten models are now available, and their specific details can be found in Table S2 in Supporting Information S1.

## 2.6. The Climatological Annual Cycle of the Indian Rainfall

The climatological annual cycle of Indian rainfall is examined in this study, comparing model simulations with observations. Figure S3 in Supporting Information S1 illustrates the annual cycle of Indian rainfall from both the model and observations. The observed climatology is derived from the CPC unified Gauge-Based analysis of global daily precipitation, which has a horizontal resolution of  $0.5^\circ \times 0.5^\circ$  (Chen et al., 2008). The observed rainfall is concentrated mainly in June–August. Eight CMIP6 models used in the CDR forcing experiment and 10 CMIP6 models employed in the AGCM simulation are analyzed. It is noted that there are notable differences among the CMIP6 models, with many tending to simulate a stronger and delayed onset of the rainy season compared to observation during the last 100 years of piControl experiment. Similar results were observed in the historical experiment (Figures are not shown; Bombardi & Boos, 2021; Sabeerali & Ajayamohan, 2017). However, three models—MIROC6, MIROC-ES2L, and CanESM5—show distinct behaviors: MIROC6 and MIROC-ES2L simulate an extreme early onset of the rainy season, while the CanESM5 exhibits much weaker rainfall intensity than observation. Therefore, these three models are excluded to provide a better characterization of the ISM onset. Consequently, the climatological onset dates in CMIP6 models are systematically late, consistent with CMIP5 simulations (Sabeerali & Ajayamohan, 2017; Sooraj et al., 2014; Sperber et al., 2013). The MME indicates an onset date of 21 June, more than half a month later than the observed onset. Despite these discrepancies, our focus is on exploring the relative changes in the onset dates of the ISM, rather than projecting a precise onset date under a CDR scenario. Therefore, the MME results can be used for informative purposes. Additionally, when exploring the underlying mechanisms, we specifically analyze the June-mean data, as the ISM onset typically occurs in mid- to late-June in CMIP6 models.

## 2.7. Statistical Tests

This paper utilized two statistical tests: the sign agreement test and the significance of the difference in the means test (Power et al., 2012; Wilks, 2019). The sign agreement test is employed to assess the robustness of the climate responses projected by MME. It determines if the sign (positive or negative) of more than 75% of the model members aligns with that of the MME. In the CDR scenario and AGCM simulations, six and eight models, respectively, are involved in the calculation of the MME (Table S2 in Supporting Information S1). Thus, to pass the sign agreement test, at least five out of six model members and six out of eight model members should have



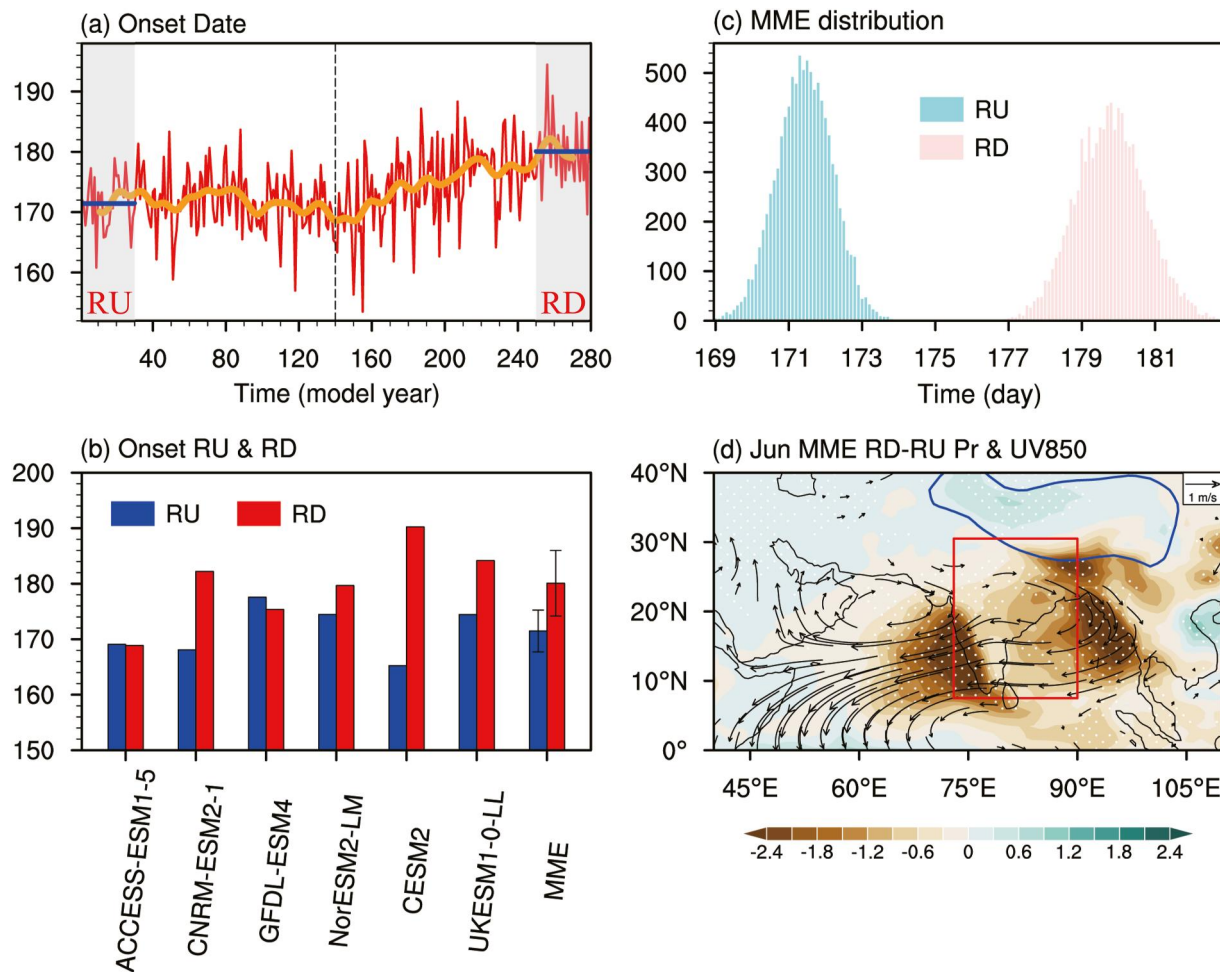


**Figure 2.** The response of ISM onset time, precipitation, and winds at 850 hPa around India to idealized CDR pathways. (a) Evolution of the ISM onset date (red line) and its 21-year low-pass filtered values using the Lanczos method (orange line) in idealized CDR experiments. Two gray shaded areas represent the RU and RD periods (both are 30-year periods) with the same average  $\text{CO}_2$  concentration. Two blue lines indicate the average ISM onset date during the RU (171.5th day; 22 June) and RD (180.1st day; 30 June) periods. The vertical dotted line represents the  $\text{CO}_2$  peak year (Year 140). (b) Comparison of the average ISM onset date during the RU and RD periods in each model and the MME. The error bars indicate the inter-model uncertainty ( $1.96 \times$  standard deviation). (c) Monte Carlo test of mean ISM onset date of MME during the RU (blue bars) and RD (red bars) periods. (d) Differences in MME precipitation (shadings; units:  $\text{mm d}^{-1}$ ) and winds at 850 hPa (vectors; units:  $\text{m s}^{-1}$ ) between the RD and RU periods in idealized CDR experiments. Dotted areas and displayed arrows indicate the results pass the sign agreement test. The red box marks the ISM region ( $7.5^\circ\text{--}30.5^\circ\text{N}$ ,  $73^\circ\text{--}90^\circ\text{E}$ ). The Tibetan Plateau is highlighted in a blue curve.

the same sign as the MME. The significance of the difference in means test is performed using the 10,000-resampling Monte Carlo bootstrap method. For the ISM onset date of MME, its values during the RU and RD periods are randomly resampled to generate 10,000 realizations of mean values for each period. These values are then sorted in ascending order. The 2.5th and 97.5th percentiles of the sorted values are selected as the lower and upper confidence bounds at the 95% confidence level, respectively. If the distributions of ISM onset date during RU and RD periods are clearly distinguishable, a statistically significant difference in the average ISM onset date between these periods is above the 95% confidence level.

### 3. Results

#### 3.1. Delayed Onset of ISM in Idealized CDR Pathway

The temporal evolution of the ISM onset date exhibits strong asymmetry in response to the idealized symmetric CDR forcing (Figure 2a). During the ramp-up period, as the  $\text{CO}_2$  concentration increases, the change in the onset date is relatively small, with a shift of approximately 2 days earlier than the PI period. However, as soon as  $\text{CO}_2$

begins to decrease in the ramp-down period, the onset date experiences a significant delay, approximately 10 days later. Hence, the application of the symmetric CDR leads to a delayed ISM onset date.

Comparing the RU (Years 1–30) phase in the ramp-up period with the same CO<sub>2</sub> concentration, four out of the six models exhibit a delayed ISM onset during the RD (Years 250–279) phase when the CO<sub>2</sub> concentration returns to its initial level (Figure 2b). In the MME, the delay in ISM onset during the RD phase amounts to more than 1 week (8.6 days). The above change is greater than its one standard deviation of the entire CDR phase (6.1 days), and the difference between the average onset dates of the RU and RD periods is statistically significant at the 95% confidence level (Figure 2c).

The onset of ISM is not only characterized by a sudden increase in precipitation but also by the firm establishment of the southwest monsoon circulation (Bombardi et al., 2020; Hu et al., 2022). The onset date of ISM exhibits a significant negative correlation with June mean precipitation and winds at 850 hPa over India throughout 280 years (Figure S4 in Supporting Information S1). In other words, an earlier onset is associated with more precipitation with anomalous westerly winds around India. To further validate the aforementioned results, Figure 2d displays the differences in June mean precipitation and winds at 850 hPa between the RD and RU periods. Compared with the RU period, the RD period is characterized by anomalous easterly winds over India, along with reduced precipitation. This finding confirms the robustness of the asymmetric response of ISM onset date to idealized CDR forcing. Therefore, if the symmetric CDR is applied, India may experience a delayed onset of the rainy season.

The onset date of ISM is delayed under idealized CDR forcing, with the reduced precipitation in June. Since the definition of ISM onset in this study is based on precipitation variable, we focus on the sudden increase in precipitation as the monsoon onset. To understand the reasons behind the decrease in June precipitation over India, we employ a simplified moisture budget equation for analysis. The decomposition of anomalous precipitation ( $\Delta P$ ) can be expressed as (P. Huang et al., 2013; Seager et al., 2010):

$$\Delta P \approx -\frac{1}{\rho g}(\Delta q \cdot \omega + q \cdot \Delta \omega) \quad (6)$$

where  $\Delta$  denotes the difference from the PI.  $q$  represents the specific humidity at 850 hPa,  $\omega$  denotes pressure velocity at 500 hPa,  $\rho$  denotes the density of water,  $g$  is the gravitational acceleration, and the last two constants are omitted hereafter for convenience. The two terms on the right-hand side of Equation 6 represent the thermodynamic ( $-\Delta q \cdot \omega$ ) and dynamic ( $-q \cdot \Delta \omega$ ) terms related to the moisture and circulation changes, respectively. Horizontal moisture advection and nonlinear processes are neglected for simplicity.

Figure 3 presents the decomposition result for the difference between the RD and RU periods. Equation 6 closely resembles the precipitation changes observed in the full models (Figures 3c and 3d), indicating its suitability as a linear approximation for tropical precipitation. The difference in the thermodynamic component (Figure 3a) between the RD and RU periods is relatively small, reflecting the “wet-get-wetter” mechanism (Held & Soden, 2006). In contrast, the dynamic component (Figure 3b) demonstrates the decreased precipitation over India, which dominates the overall rainfall changes in June. This suggests that the decreased dynamic precipitation, associated with the weakened circulation, is mainly responsible for the delayed onset of ISM during the CDR period.

### 3.2. Contributions of Fast and Slow Responses

For tropical circulation changes, the underlying SST change is a predominant driver (Ma et al., 2018; J. Ma & Xie, 2013; Xie et al., 2010). In this study, we investigate the mechanism for the decreases in dynamic precipitation associated with the weakened circulation by decomposing the climate changes into the processes driven by fast and slow SST changes (see Section 2 for details). As seen in Figure 4, the total fast response is characterized by an anomalous strong land-sea thermal gradient (i.e., stronger warming over the land than over the ocean), indicating an enhancement of the monsoonal circulation over India (Figures 4a and 5a). The enhanced circulation facilitates moisture transport, resulting in increased precipitation in June and the earlier onset of ISM (Figures 5a and 5c). The slow response is characterized by significant warming in the ocean (Figure 4b), with patterns resembling El Niño and Indian Ocean dipole (IOD) conditions over the tropical Pacific Ocean and Indian Ocean, respectively.

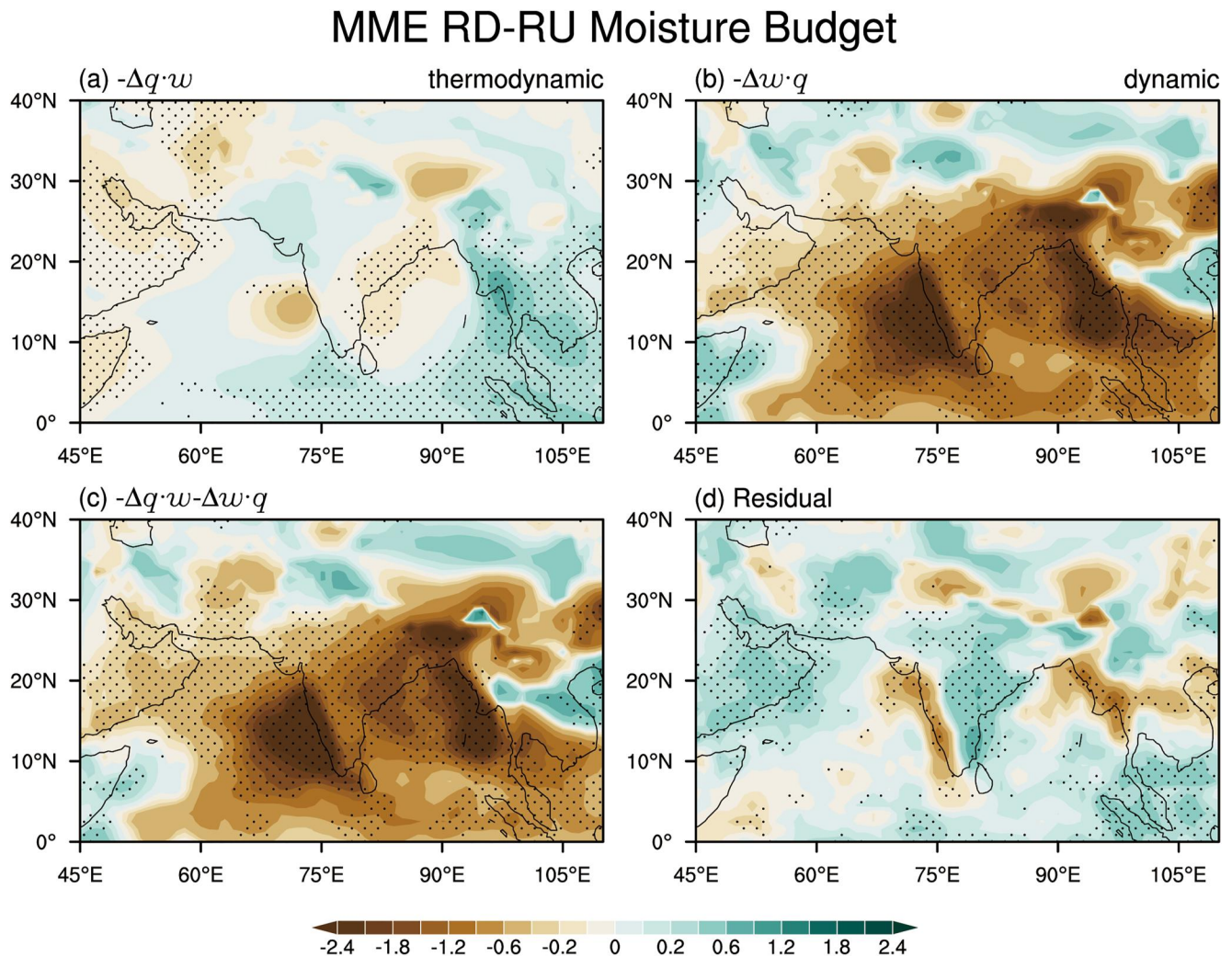


**Figure 3.** The decomposition of June mean precipitation changes (unit: mm d<sup>-1</sup>) in the RD period compared to the RU period. The changes in the thermodynamic component (a), dynamic component (b), the summation of these two terms (c), and the residual between the decomposition and Indian rainfall changes (d). Stippling indicates the values over the region pass the sign agreement test.

The slow response is associated with the weakened monsoonal circulation and a decrease in Indian precipitation, leading to the opposite effect on onset date (delayed onset) compared to the total fast response (Figures 5b and 5c).

The circulation induced by the total fast SST change advances the onset of ISM, while that caused by the slow SST change delays it. The total fast and slow responses are used to interpret the time evolution of global mean surface temperature (GMST) under the idealized CDR pathway through spatial multiple linear regression (see Section 2 for details). Figure 6a illustrates the June mean GMST changes in the idealized CDR scenario (red line), along with the estimated contributions from these two timescale processes. The contribution of the total fast response (orange line) is largely symmetric and closely synchronized with the evolution of CO<sub>2</sub> concentration (black line). It primarily influences the GMST changes during the CO<sub>2</sub> ramp-up period, with its relative contribution decreasing in time (Figure S5 in Supporting Information S1). The difference in surface temperature change and lower-level winds induced by the fast response between the RU and RD periods is negligible (Figure 6b).

In contrast, the contribution of the slow response exhibits strong asymmetry (green line in Figure 6a), lagging behind the evolution of CO<sub>2</sub> concentration. It displays a remarkable increase around the 40th year of the CO<sub>2</sub> ramp-up period and continues to increase for about 30 years after CO<sub>2</sub> peaks. Subsequently, the slow response dominates the total GMST change (Figure 6a and Figure S5 in Supporting Information S1). Around India, the



## MME Surface Temperature Response

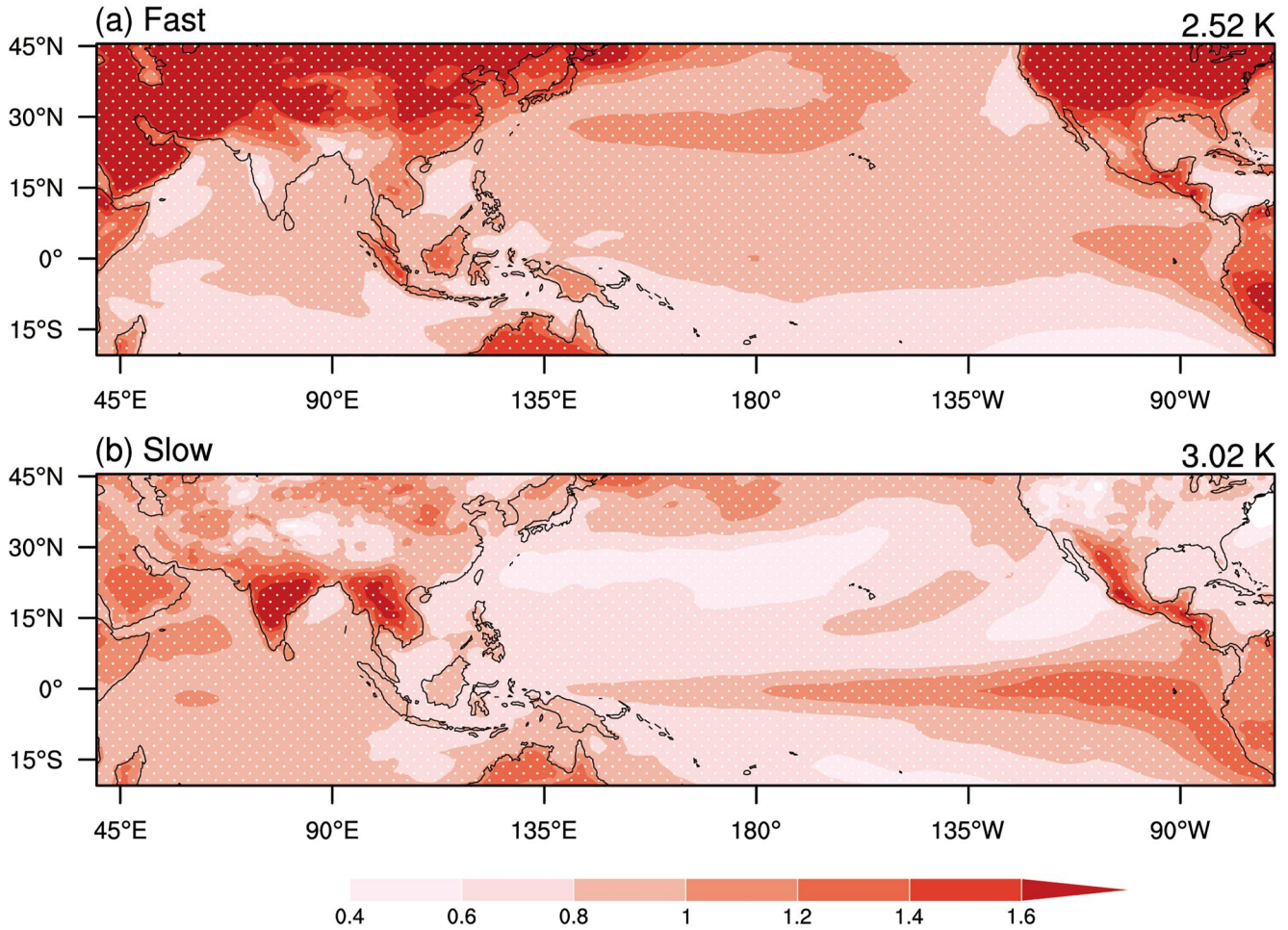


**Figure 4.** The patterns of fast (a) and slow (b) responses of surface temperature (shading; units: K K<sup>-1</sup>) in the abrupt-4 × CO<sub>2</sub> experiment. These results are normalized by dividing by the corresponding changes in global mean surface temperature (displayed in the upper right corners). White dots indicate more than 75% of ensemble members (five out of six) agree with the sign of the MME.

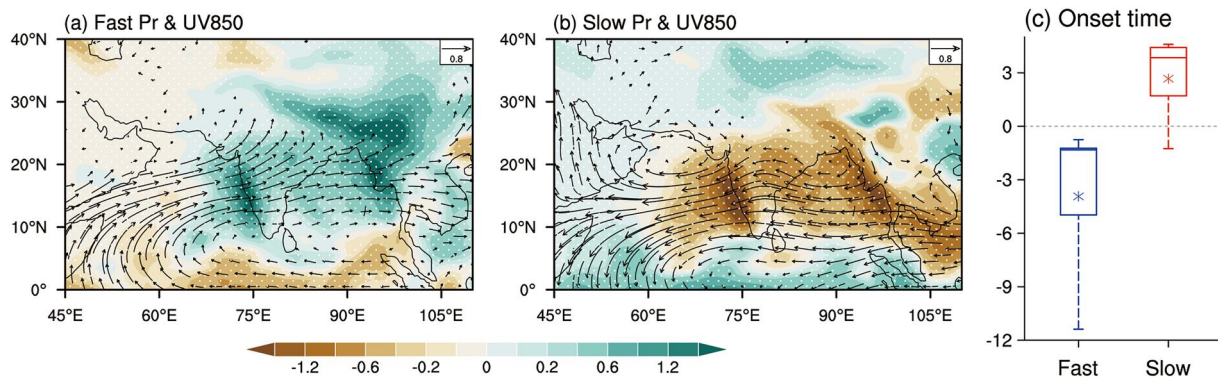


**Figure 5.** The changes in June precipitation (shading; unit: mm d<sup>-1</sup> K<sup>-1</sup>) and winds at 850 hPa (vectors; unit: m s<sup>-1</sup> K<sup>-1</sup>) due to the fast (a) and slow (b) response in the abrupt-4 × CO<sub>2</sub> experiment. The changes are responses to per 1 K of global mean surface warming. (c), as in (a, b) but for onset date change (d K<sup>-1</sup>). The boxes in (c) indicate the spread of model members (from the 25th and 75th quantiles, the center line indicates the median). The asterisks indicate the MME of six models. Stippling and displayed vectors are the same as in Figure 2d.

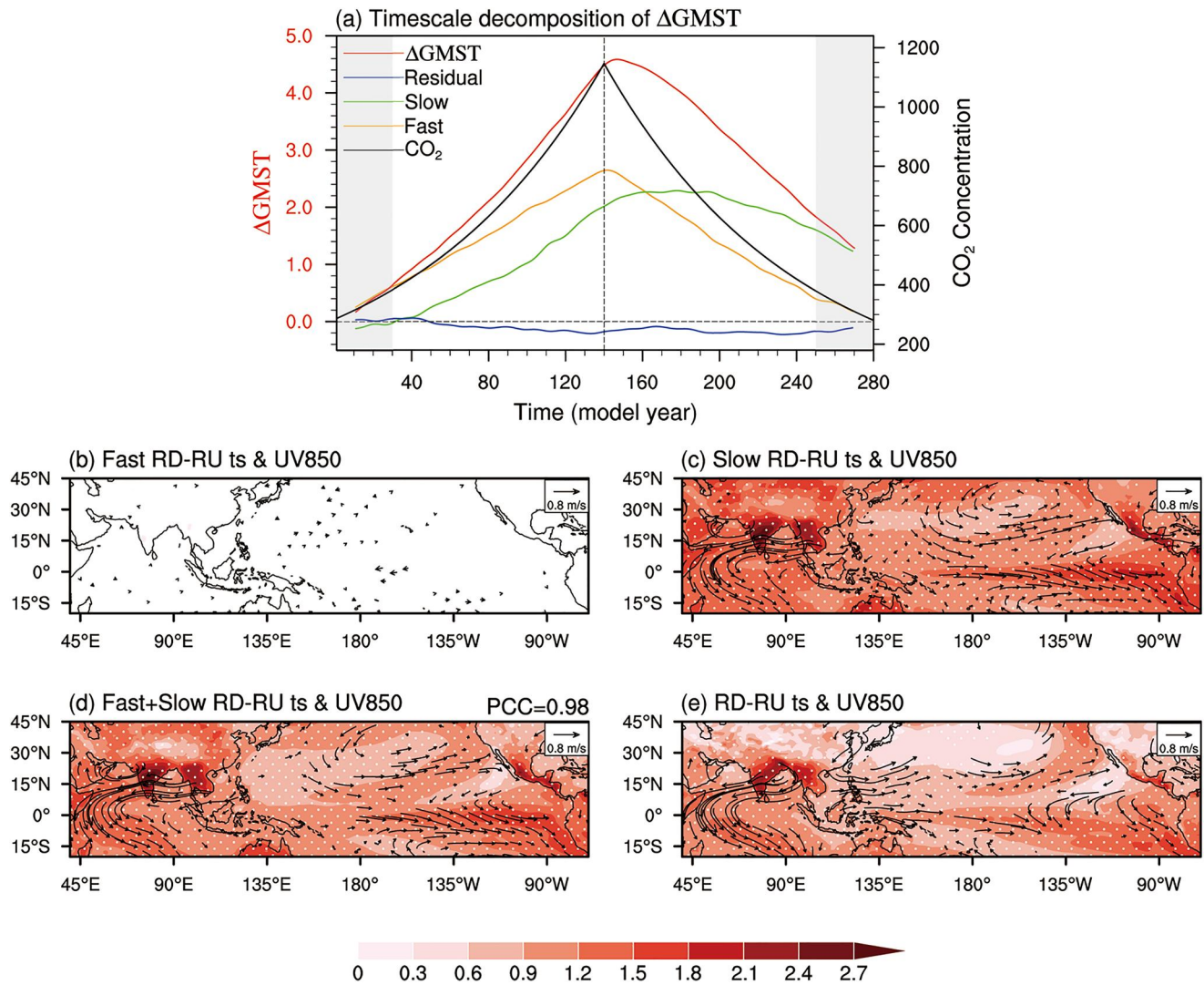


**Figure 6.** The contribution of fast and slow response in idealized CDR experiments and their differences between RD and RU periods. (a) The contribution of the fast (orange line) and slow (green line) responses to global mean surface temperature change (red line) in the idealized CDR experiments. The results are filtered using 21-year low-pass weight. The blue line represents the residual of the above timescale decomposition. Two gray shadings and the dashed vertical line are the same as in Figure 2a. The differences in fast (b), slow (c) surface temperature, and winds at 850 hPa responses between the RU and RD periods. (d) The summation of (b) and (c). (e) The difference in surface temperature and winds at 850 hPa responses between the RU and RD periods in idealized CDR forcing. The spatial correlation of surface warming between (d) and (e) is displayed in the top-right corner of (d). The white dots and vectors are the same as in Figure 2d.

circulation induced by the slow response exhibits anomalous easterly winds, corresponding to a delayed onset of ISM (Figure 6c). The residual between the results of the reconstruction and the full models is relatively low (blue line in Figure 6a), and the spatial correlation coefficient for both is high at 0.98 (Figures 6d and 6e), indicating that the decomposition approach has a good ability to reproduce GMST change, despite its limitations. The analysis indicates that the delay of the ISM onset date is primarily driven by the intensified contribution of the slow response during the CDR period. The weakened monsoonal circulation, resulting from the intensified slow surface warming (El Niño-like and IOD-like warming patterns) during the RD period compared to the RU period, delays the ISM onset.

### 3.3. Mechanism for the Delayed ISM Onset

The analysis presented above reveals that the slow response, through its influence on circulation weakening, delays the ISM onset. Additionally, its asymmetric contribution to GMST change results in asymmetric and delayed ISM onset in the idealized CDR scenario. This raises the question of how the slow response induces



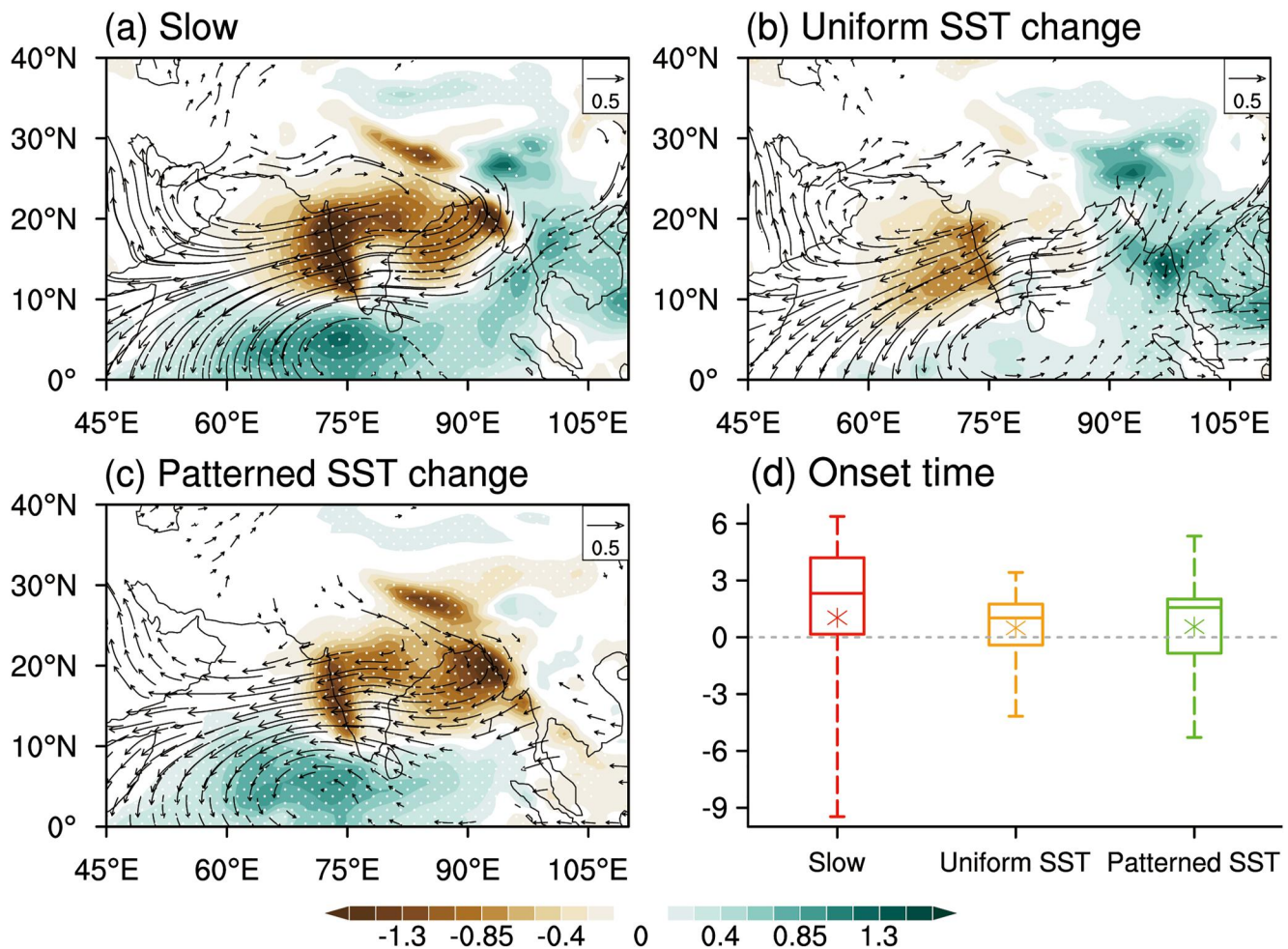


**Figure 7.** The response of precipitation (shadings; unit:  $\text{mm d}^{-1}$ ) and winds at 850 hPa (vectors; unit:  $\text{m s}^{-1}$ ) to (a) SST warming, (b) uniform SST change, and (c) patterned SST change. (d) The response of ISM onset dates to these three effects. The boxes are the same in Figure 5c. Stippling and displayed vectors are the same as in Figure 2d.

circulation changes that impact the ISM onset. To investigate this, a series of AGCM experiments, including the AMIP, AMIP-p4K, and AMIP-future4K experiments, are analyzed (See methods for details).

Based on the MME of AGCM simulations, the slow response of surface temperature driven by SST change closely resembles the results of the abrupt-4  $\times$  CO<sub>2</sub> experiment, with a spatial correlation of up to 0.9 (Figures S6a in Supporting Information S1 and Figure 4b). The surface temperature change induced by uniform SST change exhibits significant land warming; while the tropical Pacific Ocean and Indian Ocean feature El Niño-like and IOD-like warming patterns, respectively (Figures S6b and S6c in Supporting Information S1). Consequently, decreased precipitation and anomalous easterly winds occur over India, leading to a delayed ISM onset (Figure 7). Therefore, the AGCM simulations can be employed to investigate the mechanisms for the effect of slow response on ISM onset.

To assess the relative contributions of uniform SST change and patterned SST change to the delayed ISM onset in the idealized CDR scenario, the normalized responses (divided by the corresponding GMST change in the AGCM simulations) are multiplied by the MME GMST change in the RD period relative to the RU period (1.4 K). As consistently suggested by the precipitation and winds at 850 hPa (Figure 7a–7c), both uniform SST change and patterned SST change act to delay the onset of the ISM, but the latter contributes more to the overall effect of the slow response. This may be related to the effect of the increased moisture in the uniform SST change, which partially offsets the effect of the weakened circulation, resulting in a weaker change in precipitation. Due to the large inter-model uncertainty, the magnitude of the relative contribution is not noticeably distinct with respect to

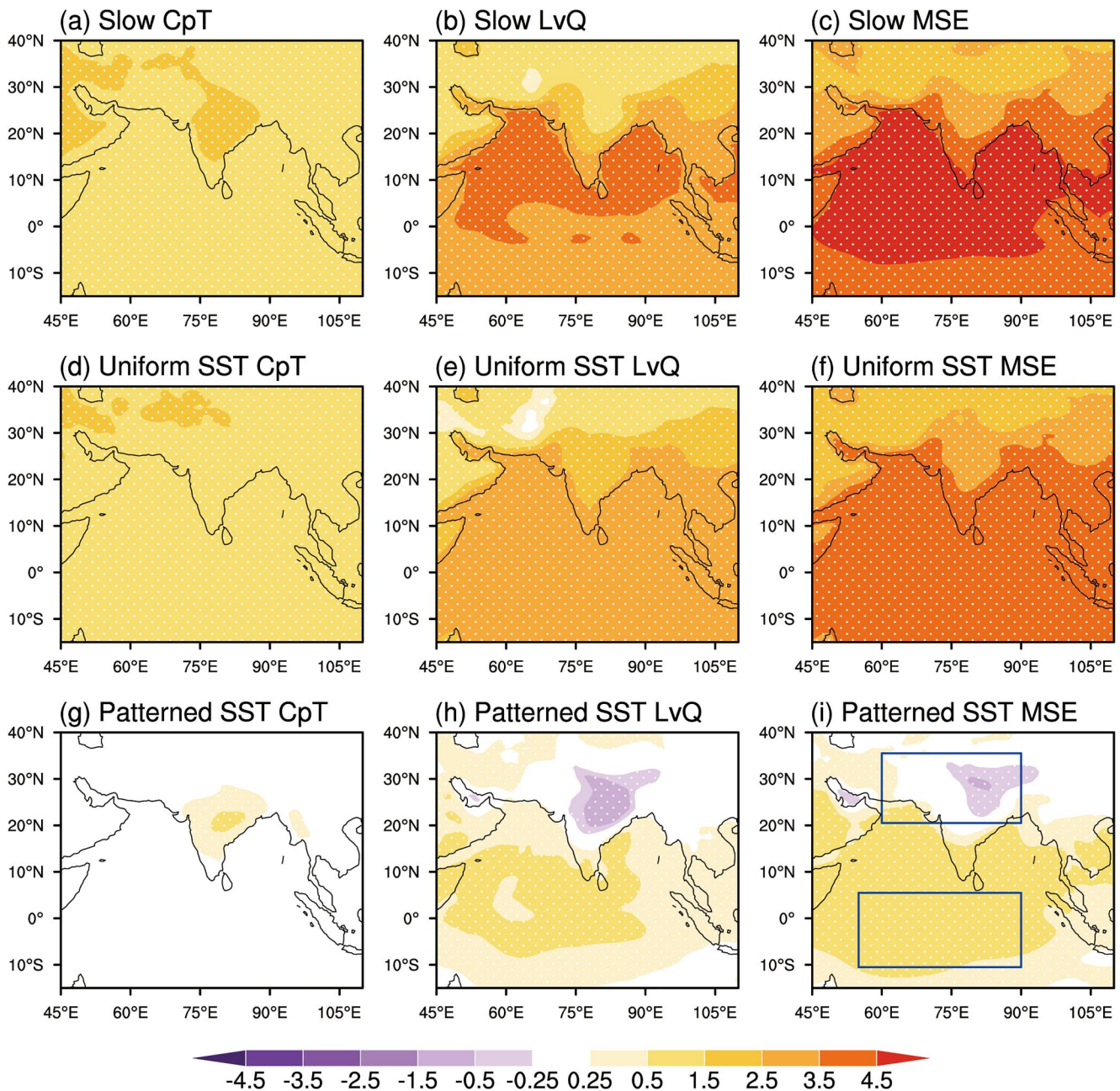


**Figure 8.** The responses of June mean near-surface air temperature in energy unit (a, d, g), specific humidity in energy unit (b, e, h), and moist static energy (c, f, i) to slow response (a, b, c), uniform SST change (d, e, f), and patterned SST change (g, h, i). The results are normalized by global mean surface warming. Units are  $\text{kJ kg}^{-1} \text{K}^{-1}$ . Stippling as in Figure 2d. The two blue boxes over the land ( $20.5^{\circ}\text{--}30.5^{\circ}\text{N}$ ,  $60^{\circ}\text{--}90^{\circ}\text{E}$ ) and Indian Ocean ( $10.5^{\circ}\text{S}\text{--}5.5^{\circ}\text{N}$ ,  $55^{\circ}\text{--}90^{\circ}\text{E}$ ) in (i) are used to define the land-sea contrast.

the MME ISM onset date, but they can be well distinguished by the median, which is not susceptible to outliers (Figure 7d). Therefore, the AGCM simulations further demonstrate that the SST pattern change plays an essential role in the slow response to delay ISM onset under the idealized CDR scenario.

How does the slow response impact the ISM onset through circulation changes? One possible explanation is the near-surface land-sea moist static energy (MSE) contrast (Bombardi & Boos, 2021; Bordoni & Schneider, 2008). The onset of monsoon is linked to the meridional shifts of the intertropical convergence zone (ITCZ), the location of which corresponds to that of the near-surface MSE maximum (Bordoni & Schneider, 2008; Hu et al., 2007; Schneider et al., 2014). As shown in Figure S7 in Supporting Information S1, before the ISM onset, the near-surface



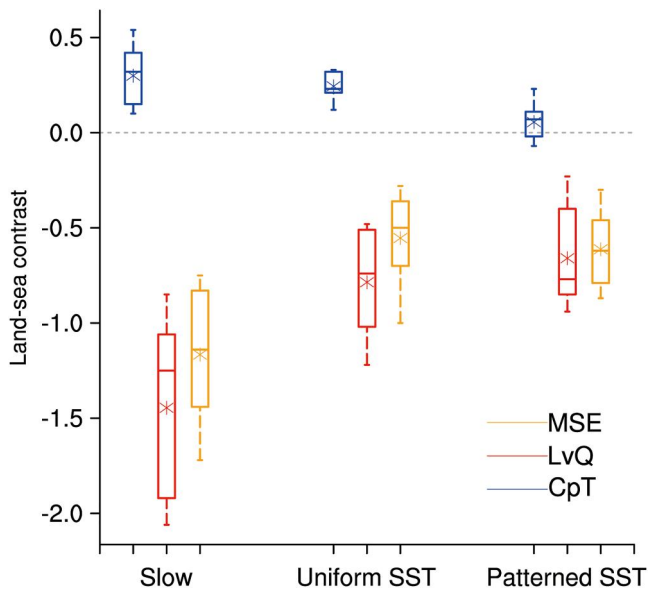


**Figure 9.** June mean land-sea contrast intensity (unit:  $\text{kJ kg}^{-1} \text{K}^{-1}$ ) for MSE-related terms in response to the slow response, uniform SST change, and patterned SST changes. The boxes are the same as that in Figure 5c.

MSE is maximum near the equator and decreases poleward. Accompanying the ISM onset, the near-surface MSE maximum shifts northwards, and the gradient of near-surface MSE is reversed. The northward migration of ITCZ corresponds to the transition of the tropical meridional overturning circulation to a monsoon pattern, with ascent in the monsoon region and descent in the southern hemisphere. The monsoonal southwesterly winds are established in the lower level due to the Coriolis force. With this in mind, we aim to analyze the near-surface MSE pattern caused by the slow response.

The MSE incorporates temperature and moisture, which is expressed as  $\text{MSE} = C_p T_{2m} + L_v q_{2m} + gZ$  (the potential energy  $gZ$  is neglected here at the near-surface level). As shown in Figure 8, in response to slow response, the Eurasian region warms more than the Indian Ocean, but the former moistens less than the Indian Ocean. This may be related to the local feedback and the hydrological cycle over land, as well as the enhanced evaporation led by the SST warming over the ocean (Byrne & O'Gorman, 2013; Joshi et al., 2007). As a result, the near-surface MSE increases more strongly over the Indian Ocean, and the reversal of the near-surface MSE gradient in the slow response is delayed. Correspondingly, the delayed transition of the tropical overturning circulation to the monsoon regime delays the onset of ISM. Both the uniform SST and patterned SST changes exhibit similar near-surface MSE pattern responses, contributing to the delayed effect of slow response on the ISM onset.

Regarding the dominant contribution of patterned SST change demonstrated by hereinbefore analysis, we evaluate the quantitative change of each term related to the near-surface MSE gradient (Figure 9). The land-sea thermal contrast increases, while the land-sea moisture contrast decrease, the latter being the primary contributor to the change in the near-surface MSE gradient. Moreover, the near-surface MSE contrast responds more strongly to the patterned SST change than to uniform SST change, consistent with the changes in June precipitation and ISM onset date (Figure 7). This further confirms that the delayed onset of ISM is primarily driven by the patterned SST change during the CDR period.

In the case of patterned SST change, the strength of the land-sea moisture contrast near the surface dominates the change in the MSE contrast (Figure 9) and subsequently delays the onset of ISM. The IOD-like warming may contributes to this local moisture. Moreover, because of equatorial wave adjustments (Neelin & Su, 2005; Xie et al., 2010), the warming in the free troposphere triggered by El Niño-like warming over the tropical Pacific spreads horizontally throughout the tropics. Based on the Clausius-Clapeyron relationship, this leads to significant moistening over the tropical ocean (Hu et al., 2021), including the Indian Ocean (Figure 8h). In contrast, the near-surface humidity decreases over India (Figure 8h), which may be partly due to the enhanced evaporation caused by strong land warming (Figure S6c in Supporting Information S1), and also may be related to the land-ocean coupling, as the ocean serves as a source of moisture for the land (Byrne & O'Gorman, 2013).

#### 4. Conclusion and Discussion

This study addresses two key questions. First, it examines the asymmetric response of ISM onset under the idealized symmetric CDR scenario. Secondly, it investigates the role of fast and slow responses in the ISM onset and explores the underlying cause based on the CMIP6 experiments. The main conclusions are summarized as follows:

1. The ISM onset change under the idealized symmetric CDR scenario is reversible but asymmetric. When the atmospheric  $\text{CO}_2$  concentration is reduced to the initial level, the ISM onset is abnormally delayed for more than 1 week. This delay corresponds to decreased June mean precipitation and anomalous easterly wind at the lower troposphere. The weakened dynamic circulation plays a dominant role in reduced precipitation.
2. The delay in ISM onset during the CDR phase is primarily driven by the enhanced slow response associated with long-term SST changes. This slow response delays the ISM onset by strengthening the poleward near-surface land-sea MSE contrast, which delays the establishment of the monsoon regime and hence weakens the monsoonal southwesterly winds at the lower troposphere. The slow response comprises both uniform SST

change and patterned SST change, both of which contribute to the delayed ISM onset, with the latter having a greater impact.

The main focus of present study is on the role of the slow annual cycle, especially, the northward shift of the intertropical convergence zone (ITCZ). In addition, the monsoon intra-seasonal oscillation (MISO) is an important trigger for the onset of ISM (Kajikawa & Wang, 2012; Taraphdar et al., 2018). For example, the interdecadal advanced monsoon onset after the mid-1990s is partly attributed to the enhanced MISO activities (Kajikawa & Wang, 2012). This is because the amplified MISO activities can trigger the monsoon onset earlier (Bhatla et al., 2016; Kajikawa & Wang, 2012; Taraphdar et al., 2018). Therefore, we examined the difference in the amplitudes of MISO between the RD and RU periods, namely, June mean standard deviations of the 10–25-day and 30–60-day filtered rainfall (Figure S8 in Supporting Information S1). The weakening of the quasi-biweekly mode and the 30–60 days oscillation during the RD period is significant, indicating that both types of MISO are suppressed. These suppressed MISO may contribute to the delayed ISM onset, but a detailed discussion on it may be beyond the ability of this manuscript. Further studies are needed to analyze in detail the role of MISO amplitude and phase.

Despite the lagging recovery of the global hydrological cycle, the ISM onset exhibits a rapid and unusual early recovery when the CO<sub>2</sub> concentration is returned to the initial level. Such delayed onset of ISM could shrink the total duration of monsoon season, affecting the total monsoonal rainfall (Goswami & Xavier, 2005; Hu et al., 2022; Xavier et al., 2007). Therefore, the response of the ISM duration will be analyzed in future work. Moreover, the delayed ISM onset may lead to precipitation deficits in the southeastern Tibetan Plateau, with potential implications for downstream water resources (Liu et al., 2019; Zhu et al., 2020). Therefore, both global and regional-scale risks should be thoroughly assessed, despite the idealized nature of our scenarios. Additionally, our findings, which indicate that the delayed onset of ISM is predominantly driven by the slow process associated with the long-term SST change, are primarily based on the decomposition of climate response into fast and slow components. However, it is important to note that this decomposition method relies on the linear assumption. These two processes cannot provide a complete depiction of climate response, although the residual in our result is minimal. Moreover, it is important to acknowledge the presence of strong biases and uncertainties in model simulations of the onset date of ISM. The model simulated ISM onset systematically late (Hu et al., 2023; Levine et al., 2013; Sperber et al., 2013). One explanation is that the model resolution is too coarse to accurately simulate ISM onset, but it is not the primary driver (Ashfaq et al., 2016; Zhang et al., 2018). A particularly large cold bias on Tibetan Plateau and Arabian Sea SST is considered critical, which reduces the land–sea thermal contrast and monsoon circulation, and hence it generates a delayed onset (Hu et al., 2023; Levine et al., 2013). Therefore, our analysis focuses solely on the relative change in the onset date based on the MME. In addition, due to the limited number of models participating in the CDR experiments, our analyses are mainly based on the six models which we currently can access. The internal variability of the models cannot be completely eliminated and the results of the MME may be model-dependent. Thus, more large ensemble simulations are needed to better investigate the climate response to CDR. Consequently, caution should be exercised when interpreting projections of the future timing of the ISM onset.

## Data Availability Statement

The CMIP6 model data used in this study are freely available from the website, <https://esgf-node.llnl.gov/projects/cmip6/>, and can also be accessed in Eyring et al. (2016) and Keller et al. (2018). The observed global land daily precipitation (Chen et al., 2008) can be downloaded from the website, <https://climatedataguide.ucar.edu/climate-data/cpc-unified-gauge-based-analysis-global-daily-precipitation>.

## Acknowledgments

This work was supported jointly by the National Natural Science Foundation of China under Grants 42141019, No. 42175055, and No. 42261144687, and the Second Tibetan Plateau Scientific Expedition and Research program under Grant 2019QZKK0102. The authors thank the World Climate Research Program's Working Group for coordinating and promoting CMIP6 and appreciate the climate modeling groups for producing and making available their model output.

## References

- Ananthakrishnan, R., & Soman, M. K. (1988). The onset of the southwest monsoon over Kerala—1901–1980. *Journal of Climatology*, 8(3), 283–296. <https://doi.org/10.1002/joc.3370080305>
- Ashfaq, M., Rastogi, D., Mei, R., Touma, D., & Ruby Leung, L. (2016). Sources of errors in the simulation of south Asian summer monsoon in the CMIP5 GCMs. *Climate Dynamics*, 49(1–2), 193–223. <https://doi.org/10.1007/s00382-016-3337-7>
- Bhatla, R., Singh, M., & Pattanaik, D. R. (2016). Impact of Madden-Julian oscillation on onset of summer monsoon over India. *Theoretical and Applied Climatology*, 128(1–2), 381–391. <https://doi.org/10.1007/s00704-015-1715-4>
- Bombardi, R. J., & Boos, W. R. (2021). Explaining globally inhomogeneous future changes in monsoons using simple moist energy diagnostics. *Journal of Climate*, 34(21), 8615–8634. <https://doi.org/10.1175/JCLI-D-20-1012.1>
- Bombardi, R. J., Kinter, J. L., & Fraumenfeld, O. W. (2019). A global gridded dataset of the characteristics of the rainy and dry seasons. *Bulletin of the American Meteorological Society*, 100(7), 1315–1328. <https://doi.org/10.1175/Bams-D-18-0177.1>

- Bombardi, R. J., Moron, V., & Goodnight, J. S. (2020). Detection, variability, and predictability of monsoon onset and withdrawal dates: A review. *International Journal of Climatology*, 40(2), 641–667. <https://doi.org/10.1002/joc.6264>
- Bordoni, S., & Schneider, T. (2008). Monsoons as eddy-mediated regime transitions of the tropical overturning circulation. *Nature Geoscience*, 1(8), 515–519. <https://doi.org/10.1038/ngeo248>
- Byrne, M. P., & O'Gorman, P. A. (2013). Link between land-ocean warming contrast and surface relative humidities in simulations with coupled climate models. *Geophysical Research Letters*, 40(19), 5223–5227. <https://doi.org/10.1002/grl.50971>
- Chadwick, R., Ackerley, D., Ogura, T., & Dommeneget, D. (2019). Separating the influences of land warming, the direct CO<sub>2</sub> effect, the plant physiological effect, and SST warming on regional precipitation changes. *Journal of Geophysical Research: Atmospheres*, 124(2), 624–640. <https://doi.org/10.1029/2018jd029423>
- Chen, M. Y., Shi, W., Xie, P. P., Silva, V. B. S., Kousky, V. E., Higgins, R. W., & Janowiak, J. E. (2008). Assessing objective techniques for gauge-based analyses of global daily precipitation [Dataset]. *Journal of Geophysical Research*, 113(D04110). <https://doi.org/10.1029/2007JD009132>
- Eyring, V., Bony, S., Meehl, G. A., Senior, C. A., Stevens, B., Stouffer, R. J., & Taylor, K. E. (2016). Overview of the coupled model inter-comparison project phase 6 (CMIP6) experimental design and organization [Dataset]. *Geoscientific Model Development*, 9(5), 1937–1958. <https://doi.org/10.5194/gmd-9-1937-2016>
- Fasullo, J., & Webster, P. J. (2003). A hydrological definition of Indian monsoon onset and withdrawal. *Journal of Climate*, 16(19), 3200–3211. [https://doi.org/10.1175/1520-0442\(2003\)016<3200a:AHDOIM>2.0.CO;2](https://doi.org/10.1175/1520-0442(2003)016<3200a:AHDOIM>2.0.CO;2)
- Field, C. B., & Mach, K. J. (2017). Rightsizing carbon dioxide removal. *Science*, 356(6339), 706–707. <https://doi.org/10.1126/science.aam9726>
- Goswami, B. N., & Xavier, P. K. (2005). ENSO control on the south Asian monsoon through the length of the rainy season. *Geophysical Research Letters*, 32(18), L18717. <https://doi.org/10.1029/2005GL023216>
- He, C., & Zhou, T. J. (2022). Distinct responses of North Pacific and North Atlantic summertime subtropical anticyclones to global warming. *Journal of Climate*, 35(24), 4517–4532. <https://doi.org/10.1175/JCLI-D-21-1024.1>
- Held, I. M., & Soden, B. J. (2006). Robust responses of the hydrological cycle to global warming. *Journal of Climate*, 19(21), 5686–5699. <https://doi.org/10.1175/JCLI3990.1>
- Hu, D., Duan, A., Tang, Y., & Yu, W. (2023). Delayed onset of the tropical Asian summer monsoon in CMIP6 can be linked to the cold bias over the Tibetan Plateau. *Environmental Research Letters*, 18(11), 114005. <https://doi.org/10.1088/1748-9326/acff79>
- Hu, K. M., Huang, G., Huang, P., Kosaka, Y., & Xie, S. P. (2021). Intensification of El Niño-induced atmospheric anomalies under greenhouse warming. *Nature Geoscience*, 14(6), 377–382. <https://doi.org/10.1038/s41561-021-00730-3>
- Hu, P., Chen, W., Wang, L., Chen, S., Liu, Y., & Chen, L. (2022). Revisiting the ENSO-monsoonal rainfall relationship: New insights based on an objective determination of the Asian summer monsoon duration. *Environmental Research Letters*, 17(10), 104050. <https://doi.org/10.1088/1748-9326/ac97ad>
- Hu, Y. Y., Li, D. W., & Liu, J. P. (2007). Abrupt seasonal variation of the ITCZ and the Hadley circulation. *Geophysical Research Letters*, 34(18), L18814. <https://doi.org/10.1029/2007GL030950>
- Huang, G., Xu, Z., Qu, X., Cao, J., Long, S., Yang, K., et al. (2022). Critical climate issues toward carbon neutrality targets. *Fundamental Research*, 2(3), 396–400. <https://doi.org/10.1016/j.fmre.2022.02.011>
- Huang, P., Xie, S. P., Hu, K. M., Huang, G., & Huang, R. H. (2013). Patterns of the seasonal response of tropical rainfall to global warming. *Nature Geoscience*, 6(5), 357–361. <https://doi.org/10.1038/Ngeo1792>
- IPCC. (2021). In V. Masson-Delmotte, P. Zhai, A. Pirani, S. L. Connors, C. Péan, S. Berger, et al. (Eds.), *Climate Change 2021: The Physical Science Basis. Contribution of Working Group I to the Sixth Assessment Report of the Intergovernmental Panel on Climate Change*. Cambridge University Press.
- Iyer, G., Ou, Y., Edmonds, J., Fawcett, A. A., Hultman, N., McFarland, J., et al. (2022). Ratcheting of climate pledges needed to limit peak global warming. *Nature Climate Change*, 12, 1129–1135. <https://doi.org/10.1038/s41558-022-01508-0>
- Jin, Q. J., & Wang, C. (2017). A revival of Indian summer monsoon rainfall since 2002. *Nature Climate Change*, 7(8), 587–594. <https://doi.org/10.1038/nclimate3348>
- Joseph, P. V., Eischeid, J. K., & Pyle, R. J. (1994). Interannual variability of the onset of the Indian-summer monsoon and its association with atmospheric features, El-Niño, and sea-surface temperature anomalies. *Journal of Climate*, 7(1), 81–105. [https://doi.org/10.1175/1520-0442\(1994\)007<0081:Ivotoo>2.0.CO;2](https://doi.org/10.1175/1520-0442(1994)007<0081:Ivotoo>2.0.CO;2)
- Joseph, P. V., Sooraj, K. P., & Rajan, C. K. (2006). The summer monsoon onset process over South Asia and an objective method for the date of monsoon onset over Kerala. *International Journal of Climatology*, 4, 1549–1555.
- Joshi, M. M., Gregory, J. M., Webb, M. J., Sexton, D. M. H., & Johns, T. C. (2007). Mechanisms for the land/sea warming contrast exhibited by simulations of climate change. *Climate Dynamics*, 30(5), 455–465. <https://doi.org/10.1007/s00382-007-0306-1>
- Kajikawa, Y., & Wang, B. (2012). Interdecadal change of the South China sea summer monsoon onset. *Journal of Climate*, 25(9), 3207–3218. <https://doi.org/10.1175/JCLI-D-11-00207.1>
- Kakatkari, R., Gnanaseelan, C., Chowdary, J. S., Parekh, A., & Deepa, J. S. (2017). Indian summer monsoon rainfall variability during 2014 and 2015 and associated Indo-Pacific upper ocean temperature patterns. *Theoretical and Applied Climatology*, 131(3–4), 1235–1247. <https://doi.org/10.1007/s00704-017-2046-4>
- Karmakar, N., & Misra, V. (2019). The relation of intraseasonal variations with local onset and demise of the Indian summer monsoon. *Journal of Geophysical Research: Atmospheres*, 124(5), 2483–2506. <https://doi.org/10.1029/2018jd029642>
- Keller, D. P., Lenton, A., Scott, V., Vaughan, N. E., Bauer, N., Ji, D. Y., et al. (2018). The carbon dioxide removal model intercomparison Project (CDRMIP): Rationale and experimental protocol for CMIP6 [Dataset]. *Geoscientific Model Development*, 11(3), 1133–1160. <https://doi.org/10.5194/gmd-11-1133-2018>
- Kim, S. K., Shin, J., An, S. I., Kim, H. J., Im, N., Xie, S. P., et al. (2022). Widespread irreversible changes in surface temperature and precipitation in response to CO<sub>2</sub> forcing. *Nature Climate Change*, 12(9), 834–840. <https://doi.org/10.1038/s41558-022-01452-z>
- Krishnamurti, T. N., & Ramanathan, Y. (1982). Sensitivity of the monsoon onset to differential heating. *Journal of the Atmospheric Sciences*, 39(6), 1290–1306. [https://doi.org/10.1175/1520-0469\(1982\)039<1290:SOTMOT>2.0.CO;2](https://doi.org/10.1175/1520-0469(1982)039<1290:SOTMOT>2.0.CO;2)
- Kug, J. S., Oh, J. H., An, S. I., Yeh, S. W., Min, S. K., Son, S. W., et al. (2022). Hysteresis of the intertropical convergence zone to CO<sub>2</sub> forcing. *Nature Climate Change*, 12(1), 47–53. <https://doi.org/10.1038/s41558-021-01211-6>
- Levine, R. C., Turner, A. G., Marathayil, D., & Martin, G. M. (2013). The role of northern Arabian Sea surface temperature biases in CMIP5 model simulations and future projections of Indian summer monsoon rainfall. *Climate Dynamics*, 41(1), 155–172. <https://doi.org/10.1007/s00382-012-1656-x>
- Li, T., Wang, Y., Wang, B., Ting, M., Ding, Y., Sun, Y., et al. (2022). Distinctive South and East Asian monsoon circulation responses to global warming. *Science Bulletin*, 67(7), 762–770. <https://doi.org/10.1016/j.scib.2021.12.001>

- Li, X., & Ting, M. (2016). Understanding the Asian summer monsoon response to greenhouse warming: The relative roles of direct radiative forcing and sea surface temperature change. *Climate Dynamics*, 49(7–8), 2863–2880. <https://doi.org/10.1007/s00382-016-3470-3>
- Liu, Y., Chen, H., Zhang, G., Sun, J., & Wang, H. (2019). The advanced South Asian monsoon onset accelerates lake expansion over the Tibetan Plateau. *Science Bulletin*, 64(20), 1486–1489. <https://doi.org/10.1016/j.scib.2019.08.011>
- Ma, J., Chadwick, R., Seo, K.-H., Dong, C., Huang, G., Foltz, G. R., & Jiang, J. H. (2018). Responses of the tropical atmospheric circulation to climate change and connection to the hydrological cycle. *Annual Review of Earth and Planetary Sciences*, 46(1), 549–580. <https://doi.org/10.1146/annurev-earth-082517-010102>
- Ma, J., & Xie, S. P. (2013). Regional patterns of sea surface temperature change: A source of uncertainty in future projections of precipitation and atmospheric circulation. *Journal of Climate*, 26(8), 2482–2501. <https://doi.org/10.1175/JCLI-D-12-00283.1>
- Misra, V., Bhardwaj, A., & Mishra, A. (2017). Local onset and demise of the Indian summer monsoon. *Climate Dynamics*, 51(5–6), 1609–1622. <https://doi.org/10.1007/s00382-017-3924-2>
- Misra, V., Bhardwaj, A., & Mishra, A. (2018). Local onset and demise of the Indian summer monsoon. *Climate Dynamics*, 51(5–6), 1609–1622. <https://doi.org/10.1007/s00382-017-3924-2>
- Mondal, S. K., An, S.-I., Min, S.-K., Kim, S.-K., Shin, J., Paik, S., et al. (2023). Hysteresis and irreversibility of global extreme precipitation to anthropogenic CO<sub>2</sub> emission. *Weather and Climate Extremes*, 40, 100561. <https://doi.org/10.1016/j.wace.2023.100561>
- Monerie, P.-A., Pohl, B., & Gaetani, M. (2021). The fast response of Sahel precipitation to climate change allows effective mitigation action. *npj Climate and Atmospheric Science*, 4(1), 24. <https://doi.org/10.1038/s41612-021-00179-6>
- Mutton, H., Chadwick, R., Collins, M., Lambert, F. H., Geen, R., Todd, A., & Taylor, C. M. (2022). The impact of the direct radiative effect of increased CO<sub>2</sub> on the West African Monsoon. *Journal of Climate*, 35(8), 2441–2458. <https://doi.org/10.1175/jcli-d-21-0340.1>
- Neelin, J. D., & Su, H. (2005). Moist teleconnection mechanisms for the tropical South American and Atlantic sector. *Journal of Climate*, 18(18), 3928–3950. <https://doi.org/10.1175/JCLI3517.1>
- Noska, R., & Misra, V. (2016). Characterizing the onset and demise of the Indian summer monsoon. *Geophysical Research Letters*, 43(9), 4547–4554. <https://doi.org/10.1002/2016gl068409>
- Pai, D. S., & Bhan, S. C. (2015). *Monsoon 2014: A report (IMD Met. Monograph No: ESSO/IMD/SYNOPTIC MET/01(2015)/17)*. India Meteorological Department, National Climate Center.
- Pai, D. S., & Nair, R. M. (2009). Summer monsoon onset over Kerala: New definition and prediction. *Journal of Earth System Science*, 118(2), 123–135. <https://doi.org/10.1007/s12040-009-0020-y>
- Power, S. B., Delage, F., Colman, R., & Moise, A. (2012). Consensus on twenty-first-century rainfall projections in climate models more widespread than previously thought. *Journal of Climate*, 25(11), 3792–3809. <https://doi.org/10.1175/JCLI-D-11-00354.1>
- Rogelj, J., Popp, A., Calvin, K. V., Luderer, G., Emmerling, J., Gernaat, D., et al. (2018). Scenarios towards limiting global mean temperature increase below 1.5°C. *Nature Climate Change*, 8(4), 325–332. <https://doi.org/10.1038/s41558-018-0091-3>
- Sabeerali, C. T., & Ajayamohan, R. S. (2017). On the shortening of Indian summer monsoon season in a warming scenario. *Climate Dynamics*, 50(5–6), 1609–1624. <https://doi.org/10.1007/s00382-017-3709-7>
- Sanderson, B. M., Xu, Y. Y., Tebaldi, C., Wehner, M., O'Neill, B., Jahn, A., et al. (2017). Community climate simulations to assess avoided impacts in 1.5 and 2°C futures. *Earth System Dynamics*, 8(3), 827–847. <https://doi.org/10.5194/esd-8-827-2017>
- Schneider, T., Bischoff, T., & Haug, G. H. (2014). Migrations and dynamics of the intertropical convergence zone. *Nature*, 513(7516), 45–53. <https://doi.org/10.1038/nature13636>
- Seager, R., Naik, N., & Vecchi, G. A. (2010). Thermodynamic and dynamic mechanisms for large-scale changes in the hydrological cycle in response to global warming. *Journal of Climate*, 23(17), 4651–4668. <https://doi.org/10.1175/2010jcli3655.1>
- Singh, D., Ghosh, S., Roxy, M. K., & McDermid, S. (2019). Indian summer monsoon: Extreme events, historical changes, and role of anthropogenic forcings. *Wiley Interdisciplinary Reviews-Climate Change*, 10(2), e571. <https://doi.org/10.1002/wcc.571>
- Sooraj, K. P., Terray, P., & Mujumdar, M. (2014). Global warming and the weakening of the Asian summer monsoon circulation: Assessments from the CMIP5 models. *Climate Dynamics*, 45(1–2), 233–252. <https://doi.org/10.1007/s00382-014-2257-7>
- Sperber, K. R., Annamalai, H., Kang, I. S., Kitoh, A., Moise, A., Turner, A., et al. (2013). The Asian summer monsoon: An intercomparison of CMIP5 vs. CMIP3 simulations of the late 20th century. *Climate Dynamics*, 41(9–10), 2711–2744. <https://doi.org/10.1007/s00382-012-1607-6>
- Tang, H., Wang, J., Hu, K., Huang, G., Chowdary, J. S., Wang, Y., et al. (2022). Increasing 2020-like boreal summer rainfall extremes over Northeast Indian subcontinent under greenhouse warming. *Geophysical Research Letters*, 49(11). <https://doi.org/10.1029/2021gl096377>
- Taraphdar, S., Zhang, F. Q., Leung, L. R., Chen, X. C., & Pauluis, O. M. (2018). MJO affects the monsoon onset timing over the Indian region. *Geophysical Research Letters*, 45(18), 10011–10018. <https://doi.org/10.1029/2018gl078804>
- Wang, B., Ding, Q. H., & Joseph, P. V. (2009). Objective definition of the Indian summer monsoon onset. *Journal of Climate*, 22(12), 3303–3316. <https://doi.org/10.1175/2008jcli2675.1>
- Wang, F., Harindintwali, J. D., Yuan, Z., Wang, M., Wang, F., Li, S., et al. (2021). Technologies and perspectives for achieving carbon neutrality. *The Innovation*, 2(4), 100180. <https://doi.org/10.1016/j.xinn.2021.100180>
- Webb, M. J., Andrews, T., Bodas-Salcedo, A., Bony, S., Bretherton, C. S., Chadwick, R., et al. (2017). The cloud feedback model intercomparison project (CFMIP) contribution to CMIP6. *Geoscientific Model Development*, 10(1), 359–384. <https://doi.org/10.5194/gmd-10-359-2017>
- Wilks, D. J. (2019). *Statistical methods in the atmospheric sciences*. Elsevier.
- Wu, P., Ridley, J., Pardaens, A., Levine, R., & Lowe, J. (2014). The reversibility of CO<sub>2</sub> induced climate change. *Climate Dynamics*, 45(3–4), 745–754. <https://doi.org/10.1007/s00382-014-2302-6>
- Wu, P., Wood, R., Ridley, J., & Lowe, J. (2010). Temporary acceleration of the hydrological cycle in response to a CO<sub>2</sub> rampdown. *Geophysical Research Letters*, 37(12), L12705. <https://doi.org/10.1029/2010gl043730>
- Xavier, P. K., Marzin, C., & Goswami, B. N. (2007). An objective definition of the Indian summer monsoon season and a new perspective on the ENSO-monsoon relationship. *Quarterly Journal of the Royal Meteorological Society*, 133(624), 749–764. <https://doi.org/10.1002/qj.45>
- Xie, S. P., Deser, C., Vecchi, G. A., Ma, J., Teng, H. Y., & Wittenberg, A. T. (2010). Global warming pattern formation: Sea surface temperature and rainfall. *Journal of Climate*, 23(4), 966–986. <https://doi.org/10.1175/2009jcli3329.1>
- Yanai, M., Li, C., & Song, Z. (1992). Seasonal heating of the Tibetan Plateau and its effects on the evolution of the Asian summer monsoon. *Journal of the Meteorological Society of Japan*, 70(1), 319–351. [https://doi.org/10.2151/jmsj1965.70.1b\\_319](https://doi.org/10.2151/jmsj1965.70.1b_319)
- Yao, T., Masson-Delmotte, V., Gao, J., Yu, W., Yang, X., Risi, C., et al. (2013). A review of climatic controls on δ<sup>18</sup>O in precipitation over the Tibetan Plateau: Observations and simulations. *Reviews of Geophysics*, 51(4), 525–548. <https://doi.org/10.1002/rog.20023>
- Yeh, S. W., Song, S. Y., Allan, R. P., An, S. I., & Shin, J. (2021). Contrasting response of hydrological cycle over land and ocean to a changing CO<sub>2</sub> pathway. *npj Climate and Atmospheric Science*, 4(1), 53. <https://doi.org/10.1038/s41612-021-00206-6>



- Zappa, G., Ceppi, P., & Shepherd, T. G. (2020). Time-evolving sea-surface warming patterns modulate the climate change response of subtropical precipitation over land. *Proceedings of the National Academy of Sciences of the United States of America*, 117(9), 4539–4545. <https://doi.org/10.1073/pnas.1911015117>
- Zhang, L. X., Zhou, T. J., Klingaman, N. P., Wu, P. L., & Roberts, M. (2018). Effect of horizontal resolution on the representation of the global monsoon annual cycle in AGCMs. *Advances in Atmospheric Sciences*, 35(8), 1003–1020. <https://doi.org/10.1007/s00376-018-7273-9>
- Zhang, S., Qu, X., Huang, G., & Hu, P. (2023). Asymmetric response of South Asian summer monsoon rainfall in a carbon dioxide removal scenario. *npj Climate and Atmospheric Science*, 6(1), 10. <https://doi.org/10.1038/s41612-023-00338-x>
- Zhang, W., Zhou, T., & Zhang, L. (2017). Wetting and greening Tibetan Plateau in early summer in recent decades. *Journal of Geophysical Research: Atmospheres*, 122(11), 5808–5822. <https://doi.org/10.1002/2017jd026468>
- Zhang, X., Zhou, T., Zhang, W., Ren, L., Jiang, J., Hu, S., et al. (2023). Increased impact of heat domes on 2021-like heat extremes in North America under global warming. *Nature Communications*, 14(1), 1690. <https://doi.org/10.1038/s41467-023-37309-y>
- Zhou, S., Huang, P., Xie, S. P., Huang, G., & Wang, L. (2022). Varying contributions of fast and slow responses cause asymmetric tropical rainfall change between CO<sub>2</sub> ramp-up and ramp-down. *Science Bulletin*, 67(16), 1702–1711. <https://doi.org/10.1016/j.scib.2022.07.010>
- Zhu, Y., Sang, Y.-F., Chen, D., Sivakumar, B., & Li, D. (2020). Effects of the South Asian summer monsoon anomaly on interannual variations in precipitation over the South-Central Tibetan Plateau. *Environmental Research Letters*, 15(12), 124067. <https://doi.org/10.1088/1748-9326/abc71b>